JACS
JOURNAL OF THE AMERICAN CHEMICAL SOCIETY
Article
pubs.acs.org/JACS

NMR-Based Conformational Ensembles Explain pH-Gated Opening and Closing of OmpG Channel

Tiandi Zhuang,[‡] Christina Chisholm,[§] Min Chen,[§] and Lukas K. Tamm*[,‡]

[‡]Department of Molecular Physiology and Biological Physics and Center for Membrane Biology, University of Virginia, Charlottesville, Virginia 22903, United States

[§]Department of Chemistry, University of Massachusetts, Amherst, Massachusetts 01003, United States

Supporting Information

ABSTRACT: The outer membrane protein G (OmpG) is a monomeric 33 kDa 14-stranded β-barrel membrane protein functioning as a nonspecific porin for the uptake of oligosaccharides in *Escherichia coli*. Two different crystal structures of OmpG obtained at different values of pH suggest a pH-gated pore opening mechanism. In these structures, extracellular loop 6 extends away from the barrel wall at neutral pH but is folded back into the pore lumen at low pH, blocking transport through the pore. Loop 6 was invisible in a previously published solution NMR structure of OmpG in *n*-dodecylphosphocholine micelles, presumably due to conformational exchange on an intermediate NMR time scale. Here we present an NMR paramagnetic relaxation enhancement (PRE)-based approach to visualize the conformational dynamics of loop 6 and to calculate conformational ensembles that explain the pH-gated opening and closing of the OmpG channel. The different loop conformers detected by the PRE ensemble calculations were validated by disulfide cross-linking of strategically engineered cysteines and electrophysiological single channel recordings. The results indicate a more dynamically regulated channel opening and closing than previously thought and reveal additional membrane-associated conformational ensembles at pH 6.3 and 7.0. We anticipate this approach to be generally applicable to detect and characterize functionally important conformational ensembles of membrane proteins.

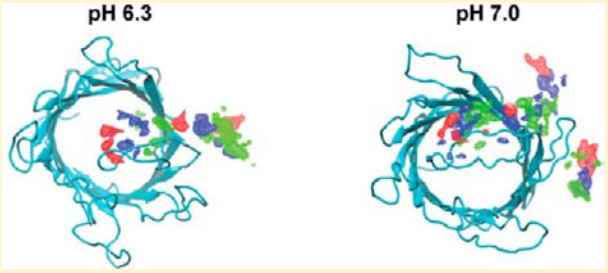

INTRODUCTION

The outer membrane protein G (OmpG) is a monomeric porin residing in the outer membrane of *Escherichia coli* where it is responsible for the uptake of sugars up to 600 Da.[1−3] The pore is large enough to pass mono-, di-, and trisaccharides but not larger oligosaccharides. OmpG expression is upregulated when the primary maltoporin LamB expression is down-regulated or in *lamB*-defective strains.[1] Permeation of sugars through OmpG is pH dependent. Single-channel recordings indicate that the open probability is much greater at neutral and slightly basic pH (7−8) than at moderately acidic pH (4.5−6).[4] High-resolution structures of OmpG in detergent micelles have been solved by X-ray crystallography and NMR,[5−7] revealing a 14-stranded β-barrel with a inner pore of 12 × 15 Å in diameter, consistent with the relatively nonspecificic uptake of saccharides up to ∼600 Da (Figure 1).

When OmpG was crystallized at pH 7.5 and 5.6 in the presence of lauryldimethylamine-*N*-oxide (LDAO) and β-D-octyl glucoside (β-OG), respectively, the two structures showed relatively constant barrel and periplasmic turn regions but significant structural changes of the extracellular loops[5] (Figure 1). At neutral pH, the loops project away from the barrel showing an open pore. At acidic pH, loop 6 folds into the pore lumen, most likely representing the closed state of the channel. This pH-regulated conformational change is believed to be triggered by two histidines (H231 in strand β12 and H261 in β13), which are in close proximity and believed to electrostatically repel each other, breaking barrel hydrogen bonds when protonated at acidic pH. To support this proposed pH-gating mechanism, a triple mutant has been engineered (called quietOmpG), in which D215 was deleted, and neighboring residues (G230 and D262) on β12 and β13 were changed to cysteines to lock the channel in the open state after disulfide bond formation.[8]

OmpG makes crystal contacts through loop 6 and other critical pore gating loops in both crystal forms. Therefore, the loop conformations could be influenced and their dynamics restricted by crystal contacts, and whether the open and closed conformations, seen in the crystal structures, also represent those of OmpG in membranes is still an open question. For example, AFM measurements showed that the extracellular loops were quite flexible in detergent micelles and lipid bilayers.[9] Consistent with the idea of flexible loops, electrophysiological single-channel measurements show that OmpG fluctuates between open and closed states and that whole populations of states, not necessarily two single rigid conformations, are shifted by pH.[4]

Received: May 31, 2013
Published: September 10, 2013

   dx.doi.org/10.1021/ja408206e | *J. Am. Chem. Soc.* 2013, 135, 15101−15113

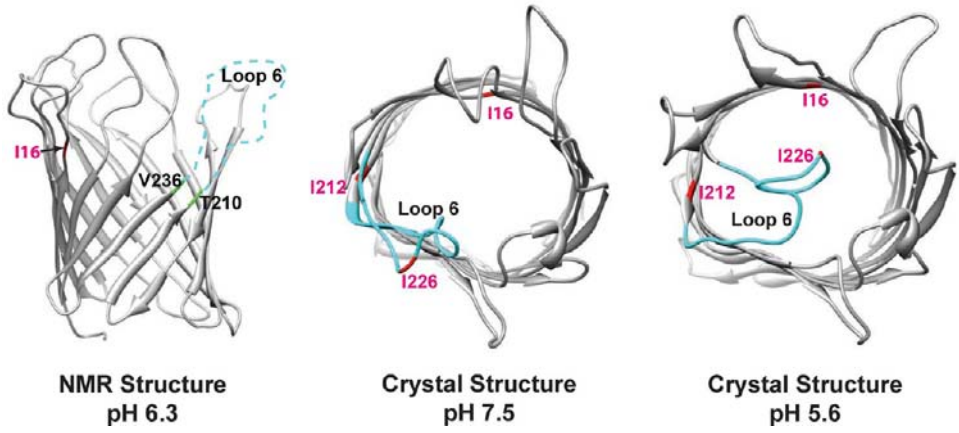

Figure 1. Ribbon representations of the structures of OmpG solved by solution NMR and X-ray crystallography showing different positions of extracellular loop 6 with respect to the pore lumen. Left: Solution NMR structure in DPC micelles at pH 6.3 (PDB: 2JQY). Loop 6 residues 211−235, shown as dashed line, are invisible by NMR. The limiting NMR-visible residues T210 and V236 are labeled. Center: Crystal structure in LDAO at pH 7.5 (PDB: 2IWV). Right: Crystal structure in βOG at pH 5.6 (PDB: 2IWW). Extracellular loops 6 are shown in cyan. The positions of the previously unassigned isoleucines I16, I212, and I226 are shown in the structures.

The solution NMR structure of OmpG in *n*-dodecylphosphocholine (DPC) micelles at pH 6.3 showed a similar β-barrel with 14 antiparallel β-strands as observed in the crystal structures, but the barrel was distinctly shorter and the loops were more disordered in the NMR than in the crystal structures.[7] Several extracellular loop residues showed broad linewidths suggesting that they were in intermediate conformational exchange under NMR conditions. Moreover, the entire loop 6, comprising residues 211−235, was invisible in the NMR spectrum. Since this loop appears to be paramount to the understanding of the pH-gating mechanism and since conformational analysis of this loop may not be accessible by traditional NMR experiments, we developed a paramagnetic relaxation enhancement (PRE)-based NMR method to characterize the conformational dynamics of the pore loops of OmpG at intermediate pH.

Nuclear relaxation enhancements arising from paramagnetic species have long been exploited in NMR, but these methods have recently gained much wider popularity in NMR of large and complex biomolecules. For example, PREs have been used for the refinement and topology mapping of membrane proteins and their interactions,[10−14] identification of sparsely populated intermediate states,[15−17] and characterizations of transient interactions.[17−19] The latter take advantage of the sixth power distance dependence ($\sim r^{-6}$) of PREs and their consequently high bias toward the closest distances in a population.[20,21]

The proposed pH-dependent shift of the conformational population equilibrium of the open and closed pore loops of OmpG makes this protein a good target for characterizing population distributions by ensemble analysis of experimental PRE data. We pursued this approach to distinguish among the different conformers and to characterize structural ensembles in the open, closed, and potentially intermediate states of OmpG. To do so, we introduced, by site-directed mutagenesis, single cysteines to multiple sites along the extracellular loops and labeled them with paramagnetic nitroxide spin probes. By analyzing the experimental PRE data in terms of conformational ensembles, we found populations of open and closed states that were similar to the corresponding crystal structures but were weighted ensembles as expected from the electrophysiological experiments. We also found an additional conformational ensemble at pH 6.3 and two more ensembles at pH 7.0. The close proximity of loops 2, 4, and 6 that emerged from the pH 6.3 closed state ensembles was confirmed by disulfide cross-linking of strategically placed cysteines and electrophysiological single-channel measurements.

MATERIALS AND METHODS

Expression, Purification, and Refolding of OmpG. Wild-type OmpG and quietOmpG (OmpG mutant carrying Δ215 and G230C/D262C) were overexpressed in *E. coli* BL21(DE3)-pLysS cells and purified using a Hitrap-DEAE anion exchange column as previously described.[7] Refolding was performed as previously described.[7] Mutants carrying single cysteine (Y22C, S58C, E101C, L141C, S182C, D224C, I226C, R228C, S266C) or double cysteines (Y22C/S182C, S58C/I226C and L141C/I226C) were constructed using the Qiagen Quickchange mutagenesis kit (Qiagen, MD). Correct plasmid sequences were confirmed by the UVA DNA sequencing facility. The expression and purification of these mutants followed the same procedures as described for wild-type with slight modifications. In brief, 5 mM dithiothreitol (DTT) was included in all buffers used in the purification and refolding protocols. The refolded protein sample was stored in a buffer containing 25 mM bis-Tris, 50 mM NaCl, 0.1 mM ethylenediaminetetraacetic acid (EDTA), 0.05% NaN_3, 5 mM DTT, pH 6.3, containing 0.5% DPC.

For residue-specific ^{15}N-labeling of isoleucine, the auxotrophic cell strain CT19, which carries the genetic lesions for the transaminases of valine, isoleucine, leucine, phenylalanine, tyrosine, and tryptophan was used.[22] Cells were grown in M9 minimal medium with ammonium chloride replaced by all 20 L-amino acids. In 1 L medium, 0.2 g ^{15}N-isoleucine and 0.2 g each of the other 19 amino acids were mixed. After adding 0.1 g/L ampicillin, 0.1 g/L kanamycin, 20 mg/L tetracycline, and 10 mL 100× MEM vitamin mix, the final medium was adjusted to pH 7.0. Cells were grown at 37 °C to OD600 = 0.8 with vigorous shaking at 250 rpm, then induced for 3−4 h using 1 mM isopropyl β-D-1-thiogalactopyranoside (IPTG). The yield of selectively labeled protein was typically 60−80 mg/L.

To adjust the pH to values other than the standard pH 6.3, OmpG was exchanged into 25 mM Na acetate, 50 mM NaCl, 0.1 mM EDTA, 0.05% NaN_3, pH 4.5, 5.0, or 5.5, containing 0.5% DPC using Amicon ultracentrifugal filters [molecular weight cut-off (MWCO) 30 kDa)]. pH 7.0 samples were prepared in 25 mM Hepes, 50 mM NaCl, 0.1 mM EDTA, 0.05% NaN_3, with 0.5% DPC. Lipid headgroup and charge effects were monitored by titrating lipopolysaccharide (Sigma, MO) or lyso-myristoyl-*sn*-glycero-3-phosphoglycerol (LMPG) (Avanti Polar Lipids, AL) to ^{15}N-OmpG prepared either at pH 6.3 or 7.0 with DPC concentration fixed at 150 mM.

Reconstitution into Bicelles. Folded OmpG in either β-OG or DPC was precipitated by isopropanol, followed by centrifugation at 10 000 rpm for 10 min. The pellet was dispersed in 500 uL detergent-free NMR buffer (25 mM bis-Tris, 50 mM NaCl, 0.1 mM EDTA, 0.05% NaN_3, pH 6.3) and spun down at 10 000 rpm for 10 min. This washing step was repeated 4−5 times to completely remove residual isopropanol and detergent. The final spin was at 13 000 rpm for 10 min. The pellet was dissolved in 300 uL 1,2-dihexanoyl-*sn*-glycero-3-phosphocholine (DHPC) containing NMR buffer (25 mM bis-Tris, 50 mM NaCl, 0.1 mM EDTA, 0.05% NaN_3 and 10% DHPC, pH 6.3). The protein was refolded by incubation in this buffer at 39 °C for at least 48 h. A $^1H-^{15}N$ TROSY spectrum was acquired and single-channel conductance measurements were performed to confirm proper refolding and function of OmpG. To make a bicelle sample (q = 0.33), the refolded protein in DHPC micelles was mixed with 15 mg 1,2-dimyristoyl-*sn*-glycero-3-phosphocholine (DMPC), followed by 4−5 freeze (0 °C, 20 min)/thaw (39 °C, 20 min) cycles until a clear solution was obtained. A more stable bicelle sample was obtained by doping the bicelle with negatively charged 1,2-dimyristoyl-*sn*-glycero-3-phospho-L-serine (DMPS) at a molar ratio of DMPC:DMPS:DHPC at 4:1:15. The formation of bicelles was confirmed by measuring rotational correlation times of protein−bicelle complexes. NMR results in bicelles with and without DMPS were equivalent. This reconstitution protocol produced bicelles with accurate q-values and reproducible correlation times.

^{15}N Relaxation Dispersion Experiments. To characterize the dynamics of extracellular loops, ^{15}N Carr−Purcell−Meiboom−Gill (CPMG) relaxation dispersion experiments were performed on OmpG at pH 7.0 at 800 MHz Bruker NMR spectrometer using the pulse scheme previously described.[23] Data were obtained at 8 CPMG frequencies ranging from 67 to 1667 Hz (T = 30 ms), including repetitions of the reference and ν_{CPMG} = 1667 Hz spectra for error estimations. CPMG dispersion profiles were analyzed using NESSY[24] and fit with two- and three-site exchange models.

Spin-Labeling and PRE Measurements. Single cysteine mutants of OmpG were labeled with (*S*-(2,2,5,5-tetramethyl-2,5-dihydro-1H-pyrrol-3-yl)methyl methanethiosulfonate (MTSL) in their unfolded, detergent-free forms. Fractions of pure OmpG from the DEAE column were pooled and concentrated to 0.5 mL by centrifugation at 3700 rpm using Amicon ultracentrifugal filters (MWCO 10 kDa). Five mM freshly made DTT was added and incubated at room temperature for 2 h to ensure fully reduced cysteines. DTT was removed by a PD-10 desalting column using a degassed urea buffer containing 10 mM Tris, 8 M urea, 0.1 mM EDTA, pH 7.0. The protein fraction was divided into two halves for paramagnetic and diamagnetic labeling. For paramagnetic spin-labeling, a 10-fold molar excess of stock MTSL was mixed with the DTT-free protein sample. The sample was covered with argon and wrapped with aluminum foil. After 30 min incubation at room temperature, a second aliquot of 10-fold molar excess of MTSL was added and incubated for another 2 h to complete the reaction. Excess MTSL was removed by a PD-10 column. The volume of the spin-labeled protein sample was reduced to <1 mL and added to 30 mL refolding buffer containing 10 mM Tris, 70 mM β-OG, 0.1 mM EDTA, pH 9.0 for refolding. Labeling with the diamagnetic acetyl analog of MTSL was performed analogously with the other half of each single cysteine mutant of OmpG. Instead of reducing the MTSL-labeled species with ascorbic acid, a direct comparison of paramagnetic and diamagnetic samples for PRE determinations avoids quantitative underestimates of PREs due to incomplete reduction.[10]

$^1H-^{15}N$ TROSY spectra of the paramagnetic and diamagnetic samples were acquired with the same NMR parameters at both pH 6.3 and 7.0. PRE enhancements for each peak were determined from the intensity ratio of the paramagnetic and corresponding diamagnetic peaks.[10] The errors were estimated by Monte Carlo simulation[25] providing the error sources from spectral signal-to-noise and small sample concentration variation leading to a scaling factor used for the intensity ratio calculation. A total of nine sets of PRE data were obtained at each pH from the different labeled sites. This resulted in 195 experimental PRE values at pH 6.3 and 232 PRE values at pH 7.0 that were used in the ensemble structure calculations.

Ensemble Structure Calculations. It was shown before[26] that the enhancement of the transverse relaxation rate R_2^{para} is insensitive to internal correlation times and that errors in effective distances resulting from ignoring internal correlation times as done in the standard Solomon−Bloembergen equation[27,28] are smaller than 4%. Therefore, PREs on transverse relaxation rates from nitroxides attached to loop residues that undergo μs−ms exchange as well as internal ps motions will not incur any significant distortions by these motions and can be treated as ensemble averages of contributions from multiple conformers following the approach of Clore and co-workers.[26] PREs were back-calculated using eq 1:

$$R_2^{para} = \frac{S(S+1)\gamma^2 g^2 \beta^2 \langle r^{-6}\rangle}{15}\left(4\tau_c + \frac{3\tau_c}{1+\omega_h^2\tau_c^2}\right) \quad (1)$$

Here, S is the electron spin quantum number, γ is the proton gyromagnetic ratio, g is the electronic g factor, β is the Bohr magneton, τ_c is the correlation time for the electron−proton interaction, and ω_h is the Larmor frequency of the proton. Ensemble-averages $\langle r^{-6}\rangle$ of amide protons were calculated by[26]

$$\langle r^{-6}\rangle = \frac{1}{N}\sum_{i=1}^{N} r_i^{-6} \quad (2)$$

When two nitroxides were attached to single cysteine, the ensemble averages were calculated as follows:[25,29]

$$\langle r^{-6}\rangle = \frac{1}{2N}\sum_{j=1}^{2}\sum_{i=1}^{N} r_{ij}^{-6} \quad (3)$$

In these equations, N represents the number of different conformers that the paramagnetic center is sampling. As previously described,[26] these ensemble calculations assume an equal and uniform transition probability $1/N$ among all N conformers, which may overlap with each other due to the exclusion of nonbonded interaction energy terms in the molecular dynamics simulation.

Ensemble structure calculations were conducted using Xplor-NIH[30,31] with an implemented PRE potential function.[26] The previously published lowest-energy NMR structure was used to generate the initial structure and topology file. The transverse relaxation rate enhancement was used in the PREpot module with r^{-6} averaging. Additional pseudo-NOE distance restraints between the backbone amide proton and the MTSL nitroxide were inserted for those residues whose peaks disappeared in the spectra of paramagnetic samples or those whose peaks had intensity ratios $I_{para}/I_{dia} > 0.9$. A distance upper bound was set at 16 Å for residues disappearing in the paramagnetic sample. A distance lower bound was set at 23 Å for residues with intensity ratio $I_{para}/I_{dia} > 0.9$. This introduced up to 976 and 957 distance restraints for samples at pH 6.3 and 7.0, respectively.

During simulated annealing, the barrel region and the periplasmic turns were fixed, and the small helix (residues 141−143) seen in crystal structure was grouped. The reason for keeping the β-barrel fixed during refinement was that the barrel was very well-defined by sufficient numbers of NOEs and hydrogen bonds in our original structure calculation.[7] A complete new refinement with all restraints in a single step could also have been done but would unlikely have changed the outcome because of the dominance of the NOE restraints in the barrel definition. The extracellular loops (defined as loop 1: residues 16−33, loop 2: residues 53−68, loop 3: residues 95−104, loop 4: residues 139−140 and 144−147, loop 5: residues 179−186, loop 6: residues 211−236, and loop 7: residues 255−272) were free to move. High-temperature dynamics were performed at 3500 K for 1 ps, followed by cooling to 100 K with 25 K per step. The force constants for PREs and NOEs were ramped to 10 and 1 kcal mol^{-1} s^2, respectively. Final minimization included a 5000 step torsion angle minimization and 5000 step Cartesian space minimization.

Ensemble sizes up to 7 and 8 were calculated at pH 6.3 and 7.0, respectively. At least 50 structures were calculated for each ensemble size, and the 30% lowest-energy structures were used for PRE back-calculations using the Solomon−Bloembergen equation. To account

for the mobility of the MTSL chain, a pseudoresidue consisting of a cysteine conjugated to two noninterfering MTSL molecules was constructed as previously described.[25,29] In this case, an ensemble size up to 4 was calculated.

Disulfide Cross-Linking. Disulfide cross-linking experiments were performed with the double cysteine mutants Y22C/S182C, S58C/I226C, and L141C/I226C and single cysteine mutants Y22C, S58C and I226C as controls. Protein samples were treated with 5 mM DTT for 2 h at room temperature. DTT was then removed by passing proteins through a PD-10 column using an EDTA-free elution buffer (25 mM Bistris, 50 mM NaCl, pH 6.3, containing 0.5% DPC). The eluted protein was diluted with EDTA-free buffer to a final concentration of 0.1 mM. Five mM copper phenanthroline was added to catalyze disulfide formation of nearby cysteines. Copper phenanthroline was freshly made by mixing $CuSO_4$ with phenanthroline at a molar ratio of 1:2. After 25 min at room temperature, the reaction was stopped by adding 20 mM EDTA. Ten μg of protein samples were mixed with β-mercaptoethanol-free running buffer and run on a 10−20% precast sodium dodecyl sulfate polyacrylamide gel electrophoresis (SDS-PAGE) bis-Tris gel (Bio-Rad, CA). The gel was stained with Coomassie blue and destained with 50% methanol and 10% acetic acid.

In-Gel Digestion and Mass Spectrometry. Gel bands of interest were cut out, transferred to a siliconized tube, washed, and destained in 200 μL 50% methanol for 3 h. The gel pieces were dehydrated in 100 μL acetonitrile and dried by vacuum centrifugation. They were rehydrated in 20 ng/μL trypsin in 50 mM ammonium acetate pH 6.8 on ice for 10 min. The samples were digested overnight at 37 °C. Excess enzyme solution was removed, followed by addition of 20 μL 50 mM ammonium acetate. The peptides were extracted from the polyacrylamide gel into 2 × 30 μL aliquots of 50% acetonitrile/5% formic acid. These extracts were combined, and their volume was reduced to 15 μL by evaporation for MS analysis.

LC-MS analysis was conducted with a Thermo Electron Orbitrap Velos ETD mass spectrometer equipped with a Protana nanospray ion source and interfaced to a self-packed 8 cm × 75 μm i.d. Phenomenex Jupiter 10 μm C18 reversed-phase capillary column. One μL aliquot of the extract was injected, and the peptides were eluted from the column by an acetonitrile/0.1 M acetic acid gradient at a flow rate of 0.5 μL/min over 0.5 h. The nanospray ion source was operated at 2.5 kV. The digest was analyzed using the data-dependent capability of the instrument acquiring full scan mass spectra to determine peptide molecular weights followed by product ion spectra to determine amino acid sequence in sequential scans.

Electrophysiological Current Recording in Planar Lipid Bilayers. Copper phenanthroline-treated S58C/I226C mutant OmpG with an intramolecular S58C-S-S-I226C disulfide bond was separated from intermolecularly disulfide-bonded dimers by Superdex-200 size-exclusion chromatography. Fractions containing pure monomers were pooled and adjusted to a final concentration of 0.5 mg/mL. Single-channel currents were recorded at room temperature in planar lipid bilayers at pH 8.5 under an applied voltage of ±50 mV as previously described.[3,8] Current recordings with wild-type OmpG were performed in parallel for comparison. Five mM DTT was added to both chambers of the mutant sample and gently stirred for 5 min, after which time single channel currents of the reduced samples were recorded. Data were collected from 20 individual wild-type and mutant proteins in the oxidized and reduced forms.

RESULTS

pH Titration Reveals a Change of the Dynamics of Loop 6. Residues 211−235 of loop 6 of OmpG were invisible in a previous NMR study, which was conducted at the intermediate pH 6.3, presumably because the loop underwent conformational exchange on a time-scale on the order of milliseconds.[7] To prove that some residues in this and other loops undergo exchange on a sub-ms time scale, we recorded relaxation dispersion data of some well-resolved peaks and found exchange rates on the order of 1500−2500 s^{-1} (Supporting Figure 1). In an attempt to obtain assignments of some additional loop 6 residues, we selectively labeled OmpG with ^{15}N-isoleucine. Isoleucine was chosen because OmpG has a total of 7 isoleucines, and only 4 of them (I10, I45, I114, and I193) were previously assigned. Isoleucines 212 and 226 are located in loop 6 and isoleucine 16 is in loop 1 (Figure 1). When OmpG was expressed in auxotrophic CT19 cells in the presence of ^{15}N-isoleucine, the expected number of 7 peaks was observed. Figure 2 shows overlaid ^{1}H−^{15}N TROSY

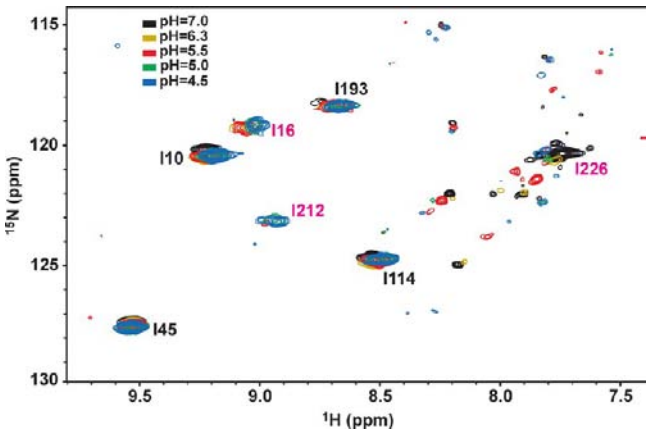

Figure 2. ^{1}H−^{15}N TROSY spectra of selectively ^{15}N-isoleucine-labeled OmpG at five values of pH (pH 7.0: black, pH 6.3: yellow, pH 5.5: red, pH 5.0: green, and pH 4.5: blue). Resonances of previously assigned isoleucines I10, I45, I114, and I193 are labeled in black. Resonances of newly assigned isoleucines I16, I212, and I226 are labeled in magenta.

spectra of ^{15}N-Ile-OmpG at 5 different values of pH. At pH 6.3, the 4 previously assigned Iles were observed as intense signals, and 2 more peaks with much weaker intensities were also evident. At pH 7.0, most isoleucine peaks decreased their intensity, but the new peak at ^{1}H chemical shift 7.7−7.8 ppm gained intensity. Another new peak at ^{1}H chemical shift 8.9−9.0 ppm became apparent only at pH values below 5.5. Finally, a third new peak appeared at most pH values around ^{1}H chemical shift 9.0−9.1 ppm. Unambiguous assignments of the three previously unassigned isoleucines were obtained through sequential site-directed mutagenesis to alanines to remove individual corresponding isoleucine peaks from the spectra. The final assignments are shown in Figure 2.

The ^{1}H chemical shifts of most isoleucines were larger than 8.5 ppm, a typical region for residues from β-strands. Even though I16 and I212 also have low-field chemical shifts (>8.5 ppm) and therefore may adopt a β-strand conformation, their peak intensities were much weaker than those of the other residues in this region, suggesting that they may undergo intermediate exchange. Indeed, these residues are in the interfacial region of OmpG where the strands transition into loops in the NMR structure and where we also observed severe line broadening in the NMR spectra of many other residues.[7]

I226 was in a chemical shift region that most likely indicates disordered structure and also exhibits the most drastic intensity change in response to pH. In contrast to the other isoleucines, the I226 TROSY cross-peak increased in intensity with increasing pH. This is consistent with I226 becoming increasingly more dynamic as the pH increases. Knowing the assignment of I226, we were able to sequentially assign five intense previously unassigned peaks in a uniformly ^{15}N-labeled

dx.doi.org/10.1021/ja408206e | J. Am. Chem. Soc. 2013, 135, 15101−15113

sample at pH 7.0 using traditional 3D sequential backbone assignment methods (data not shown). These residues were Q223, D224, D225, I226, and E227 directly following W222. All of these residues had chemical shifts consistent with a disordered structure in this region. Therefore increasing the pH only moderately from pH 6.3 to 7.0 further mobilizes the dynamic loop 6, which appears to be in contradiction to the highly ordered state of these residues in the pH 7.5 crystal structure.

PRE Measurements and Ensemble Calculations in DPC Micelles. Although the pH titration experiments revealed a fast-exchanging segment in loop 6 at pH 7.0, it is unclear whether this change in dynamics was due to a structural rearrangement in loop 6 or a shift in population between two or more dynamic conformations at different values of pH. To address this problem, we used an ensemble approach to model the spatial distribution of the extracellular loops using PREs arising from nitroxide spin-labels that were placed at nine different positions distributed over the seven extracellular loops. Figure 3A shows the nine individually spin-labeled sites in the

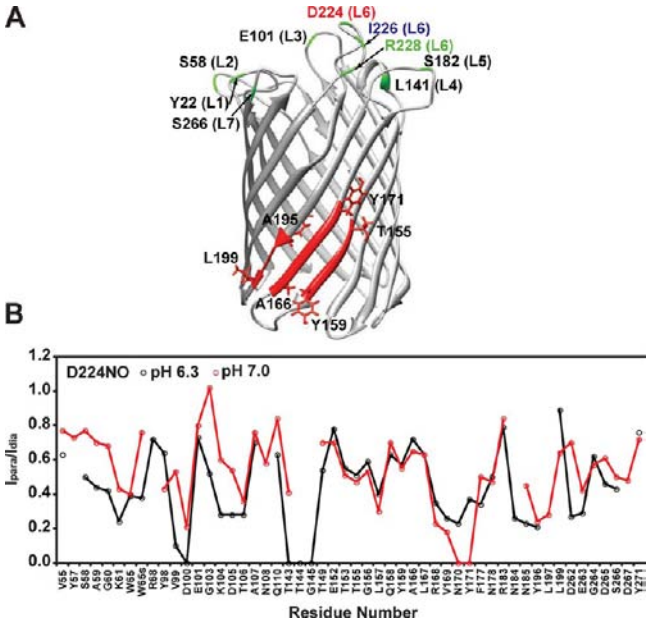

Figure 3. (A) Nine single cysteine mutation sites used for nitroxide spin-labeling in the seven extracellular loops designated Lx of OmpG. The three loop 6 mutations are labeled in color. The red highlighted barrel regions (T155-Y159, A166-Y171, and A195-L199) were strongly affected by D224NO and R228NO in DPC but not in lipid bicelles (see text). (B) Intensity ratios I_{para}/I_{dia} for $^{1}H-^{15}N$ TROSY cross-peaks affected by D224NO at pH 6.3 and 7.0 (black and red, respectively). Only residues with ratios between 0.2 and 0.8 are typically plotted, but when this value was in this range only at one pH, the corresponding ratio at other pH is also plotted for comparison.

pH 7.5 crystal structure. We engineered one single cysteine mutant for attachment of a nitroxide probe in each loop, except for loop 6 where we chose three different labeling sites. None of these mutations significantly perturbed the structure of OmpG as confirmed by 2D $^{1}H-^{15}N$ TROSY spectroscopy and electrophysiological experiments. (The additional mutant T143C resulted in a partially misfolded protein that was not further pursued. T143 is located within a small α-helix in loop 4, whose function is not clear but that might be important for proper folding of OmpG.) PRE data were collected for the nine labeled and refolded proteins in DPC at pH 6.3 and 7.0. The experimental paramagnetic/diamagnetic intensity ratios of affected peaks are shown in Figure 3B for the example of D224NO (we designate nitroxide labeled Cys residues by NO) and in Supporting Figure 2 for the other eight spin-labeled proteins. The affected peaks generally lie within a shell from ~15 to 22 Å from the nitroxides.

To analyze these data, the PREs were treated as the averages of different ensemble states such that the contribution by each ensemble state to the observed PRE average can be back-calculated from the Solomon–Bloembergen equation (see Materials and Methods). To do so, we increased the ensemble size N from 1 until the PRE Q-factor[26] no longer significantly changed. Figure 4A shows plots of PRE Q-factors versus N at pH 6.3 and 7.0. The Q-factor was quite large when a single structural ensemble was considered at either pH. The large Q-factor was also evident from the poor correlation between the experimental and back-calculated PREs using a single ensemble (Figure 4B). At pH 6.3, the Q-factor dropped to ~0.2 at $N = 3$ and did not further improve at $N > 3$ (Figure 4A). Figure 4B also shows the much better experimental/back-calculated PRE correlation at $N = 3$. A treatment with two nitroxide label conformations on a single cysteine following a previously described method[25] showed a similar trend of the PRE Q-factor reduction at pH 6.3, suggesting that we are observing by both methods backbone and not internal spin label motions. At pH 7.0, a minimum of 4 ensemble states was required to best fit the data. The result that more than one conformational ensemble was required to model the experimental PRE data is consistent with the conclusion from the pH titration, which indicated that the changing motional flexibility of loop 6 cannot be represented by a single ensemble.

Figure 5A shows the 15 lowest-energy ensemble structures of OmpG at pH 6.3 calculated from the PRE data with $N = 3$. The conformational distributions of the extracellular loops were bundled in three different conformational groups as visualized with three different colors and by viewing the molecule along the barrel axis from the extracellular side. A different representation of the same data is shown in Figure 5C. Here, the statistical distribution of structures within each ensemble was visualized using weighted atomic density maps[32] specified for D224 (red), I226 (blue), and R228 (green), which represent the three nitroxide-labeled residues in loop 6. It is clear that loop 6 samples a large conformational space. It reaches into the pore lumen in conformer 1, is roughly extended above the barrel wall in conformer 2, and folds back toward the detergent micelle in conformer 3. In marked contrast, loops 4 and 5 showed relatively small degrees of structural heterogeneity with all 3 conformers essentially superimposed on each other in the entire ensemble. This result nicely agrees with the crystallographic result showing that loops 4 and 5 did not change much between the proposed open and closed states of the OmpG channel. Loops 1–3 and 7 were intermediate between these two extremes and sampled fairly large spaces in the three conformers (Figure 5A,B). It is interesting to note that loops 2 and 6 undergo concerted conformational changes. When loop 2 moves inward toward the pore lumen (conformers 1–3), loop 6 moves outward (Figure 5B). These motions observed here at a single pH and in a single detergent environment resemble the differences observed between the proposed closed and open states obtained by crystallography from crystals grown in two different detergents and at two different values of pH. Ensemble

dx.doi.org/10.1021/ja408206e | J. Am. Chem. Soc. 2013, 135, 15101–15113

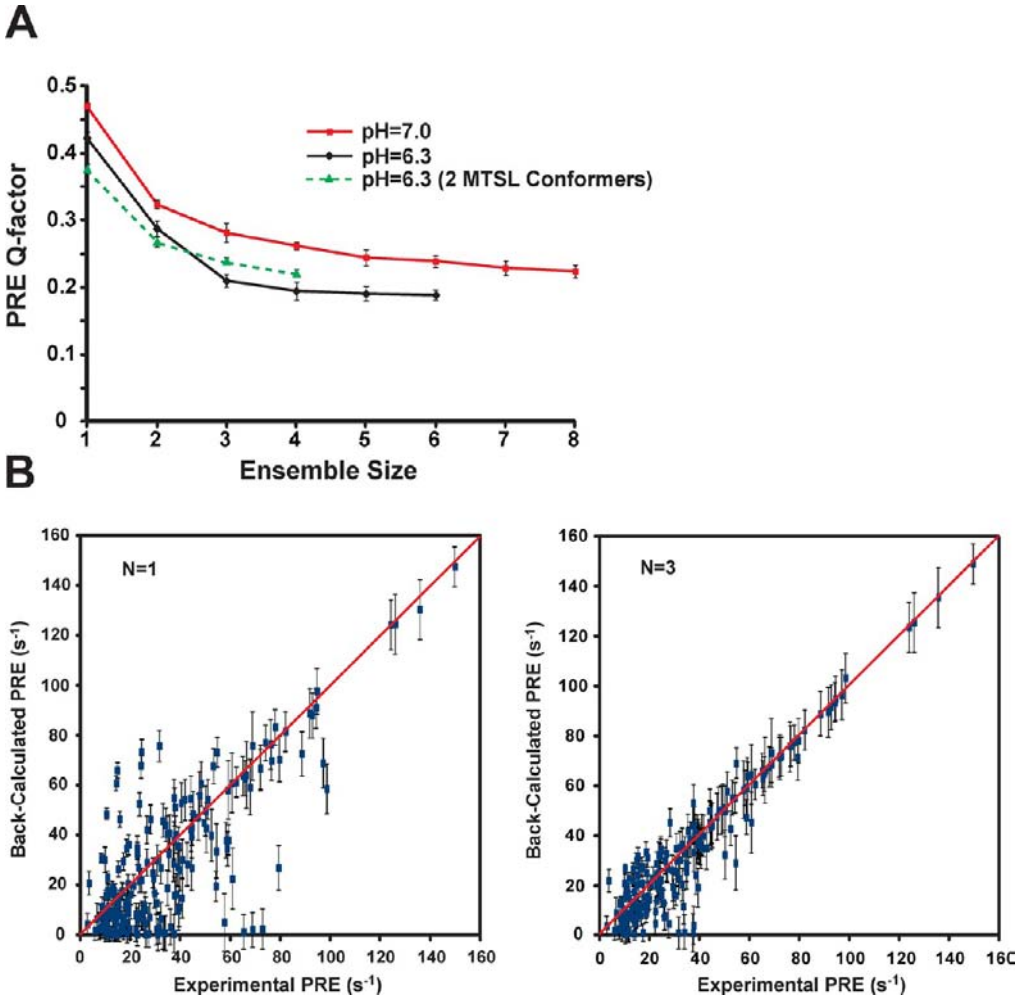

Figure 4. PRE Q-factors as function of structural ensemble size N. Q-factors were calculated using $Q = ((\sum(R_2^{obs} - R_2^{cal}))^2/(\sum(R_2^{obs})^2))^{1/2}$, where R_2^{obs} are the experimental PREs and R_2^{cal} are the back-calculated PREs using the calculated ensemble structures. (A) PRE Q-factor versus ensemble size. Black: pH 6.3 with MTSL treated as a single conformer. Green: pH 6.3 with MTSL treated as two conformers. Red: pH 7.0. (B) Correlation plots of back-calculated PREs versus experimental PREs for all PREs measured at pH 6.3 with N = 1 and 3 (left and right, respectively).

conformer 1 likely represents the closed state and ensemble conformers 2 and 3 two forms of the open state of the OmpG channel.

We also compared the experimental paramagnetic contribution to the transverse relaxation rates R_2^{para} with the sum of those separately calculated back from each ensemble conformer. Figure 5D shows these results for D224NO. Some of the relaxation enhancements were dominated by conformers 1 and 2, whereas others were dominated by conformer 3. Perhaps a little surprisingly, we observed significant relaxation enhancements for portions of three strands in the barrel region, meaning that D224 visits quite frequently the vicinity of barrel residues 155−159, 166−171, and 195−199 (highlighted in Figure 3A). We next explored whether this unusual conformational sampling of loop 6 in conformer 3 could be an artifact of the DPC micelle and whether this conformer could be suppressed in isotropic lipid bicelles that have larger elliptical bilayer-like shapes.

PRE Measurements in Lipid Bicelles. Isotropic lipid bicelles are thought to be better mimics of lipid bilayers than detergent micelles due to the presence of bilayered phospholipids surrounding the protein. Even though the sizes of isotropic bicelles are substantially larger than those of most micelles, they are suitable and their application is promising in solution NMR, as long as the long-to-short chain lipid ratios, i.e., their q-values are kept below ∼0.4, guaranteeing overall rotational correlation times that do not exceed ∼100 ns. To determine whether bicellar phospholipids suppress loop 6 interaction with the barrel wall of OmpG, we re-examined PREs in q = 0.33 bicelles composed of DMPC:DHPC = 1:3, at a protein-to-total lipid molar ratio 1:400. The particle correlation time measured by a ^{1}H-TRACT experiment[33] increased from 33 to 55 ns for OmpG in DPC micelles and isotropic bicelles, respectively (Supporting Figure 3), suggesting a molecular mass >150 kDa of the OmpG-bicelle complex. The ^{1}H−^{15}N TROSY spectrum of OmpG in isotropic bicelles was almost identical to that in DPC micelles (Figure 6A), suggesting only minor structural differences in the two media, meanwhile facilitating the resonance assignments of more than 140 peaks by correlation with assignments obtained in DPC micelles.

The PRE measurements of D224NO and R228NO were repeated in bicelles (Figure 6B). The PREs of several residues were dramatically changed in bicelles compared to micelles. Whereas R168, V169, N170, Y172, Y196, and L197 of D224NO-OmpG showed strong relaxation enhancements in micelles, these residues had much larger I_{para}/I_{dia} ratios in bicelles. Similar patterns were observed with R228NO. Although the relaxation enhancement was much less for these

dx.doi.org/10.1021/ja408206e | J. Am. Chem. Soc. 2013, 135, 15101−15113

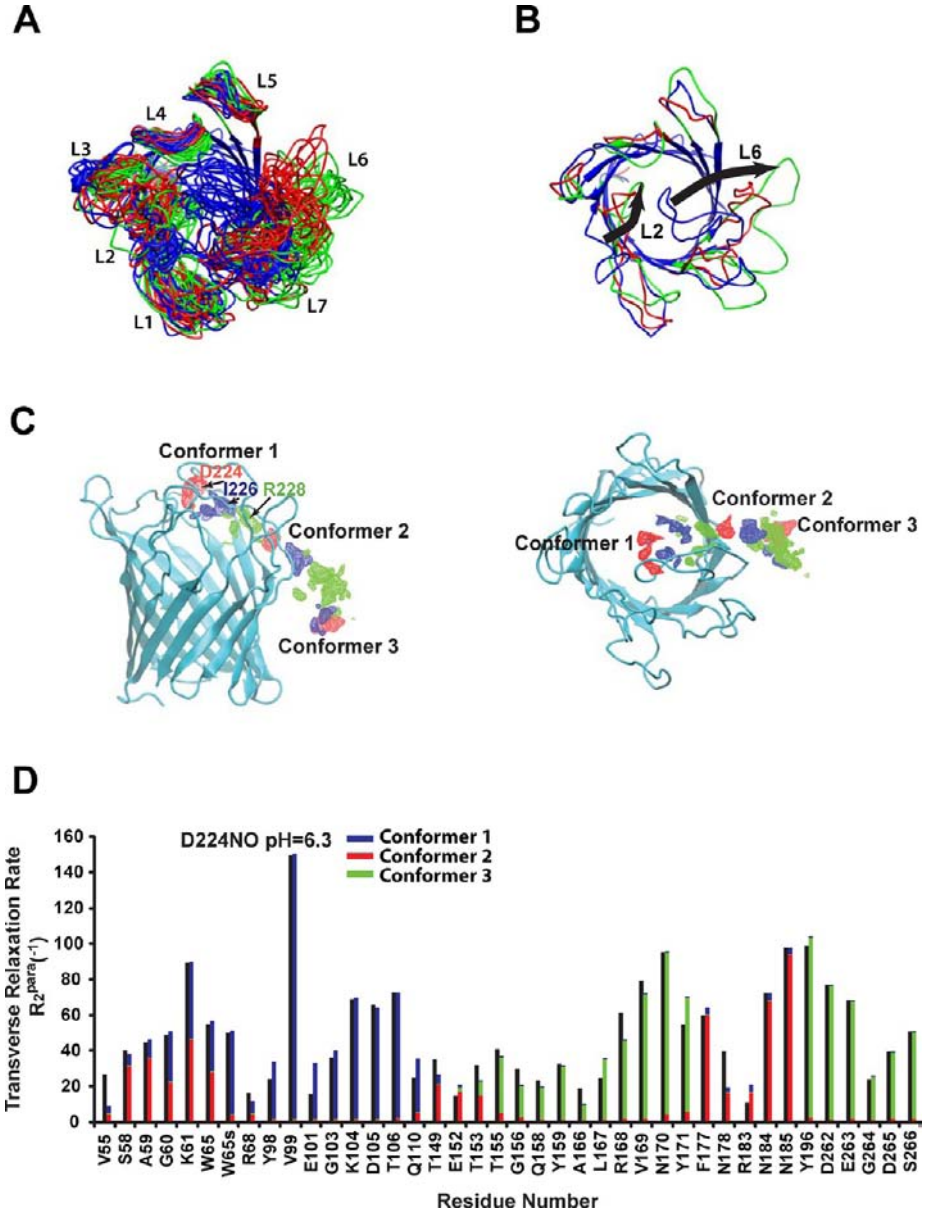

Figure 5. (A) The 15 lowest-energy ensemble structures of OmpG in DPC micelles at pH 6.3 calculated from the PRE data with $N = 3$ as viewed from extracellular side. The 3 ensemble conformers are colored blue, red, and green for conformers 1−3, respectively, based on the relative positions of I226. The approximate positions of the seven extracellular loops are labeled. (B) Backbone representation of lowest energy conformers 1−3. Same color representation as in panel A. The concerted motions of loops 2 and 6 in the three conformers are highlighted with arrows. (C) Weighted density maps of D224 (red), I226 (blue), and R228 (green) superimposed on the NMR structure of OmpG (2JQY). The densities partitioned into the three labeled ensemble conformers. Conformers 2 and 3 overlap in the projection view on the right. (D) Experimental paramagnetic contributions to transverse relaxation rates R_2^{para} (black bars) and the back-calculated R_2^{para} of D224NO. The back-calculated R_2^{para} from conformers 1−3 are colored in blue, red, and green, respectively.

residues in bicelles, we still observed I_{para}/I_{dia} substantially <1.0 for these residues in bicelles. Therefore, back-bending of loop 6 and its interaction with the barrel were less pronounced but not completely eliminated in bicelles. Extrapolation of these results to OmpG in lipid bilayers suggests that loop 6 may transiently associate with the membrane surface in its natural environment. Regardless of the exact nature of these interactions in bilayers, it is clear that the extreme back-bending of ensemble conformer 3 was probably the result of the small size and high curvature of DPC micelles. Data very similar to those in the DMPC:DHPC bicelles were obtained in DMPC:DMPS:DHPC = 4:1:15 bicelles (not shown), demonstrating that a small amount of negatively charged lipid had essentially no effect on the loop conformations in these bicelles. Details of the effect of the more complex negatively charged lipopolysaccharide (LPS) and LMPG on OmpG in DPC micelles are described in the next section.

LPS May Have No Specific Effect on the Conformation of OmpG. The major lipid on the outer surface of the outer membrane of *E. coli*, i.e., from where the loops project *in vivo*, is LPS. LPS is a complex lipid with 6 acyl chains and an inner and outer core of mostly acidic carbohydrates. In order to test whether LPS has any effect on the structure of OmpG, we titrated increasing amounts of LPS into the DPC samples (Supporting Figure 4). As a control for a much less complex acidic lipid, we added 2 mM LMPG to a DPC sample. Both

dx.doi.org/10.1021/ja408206e | J. Am. Chem. Soc. 2013, 135, 15101−15113

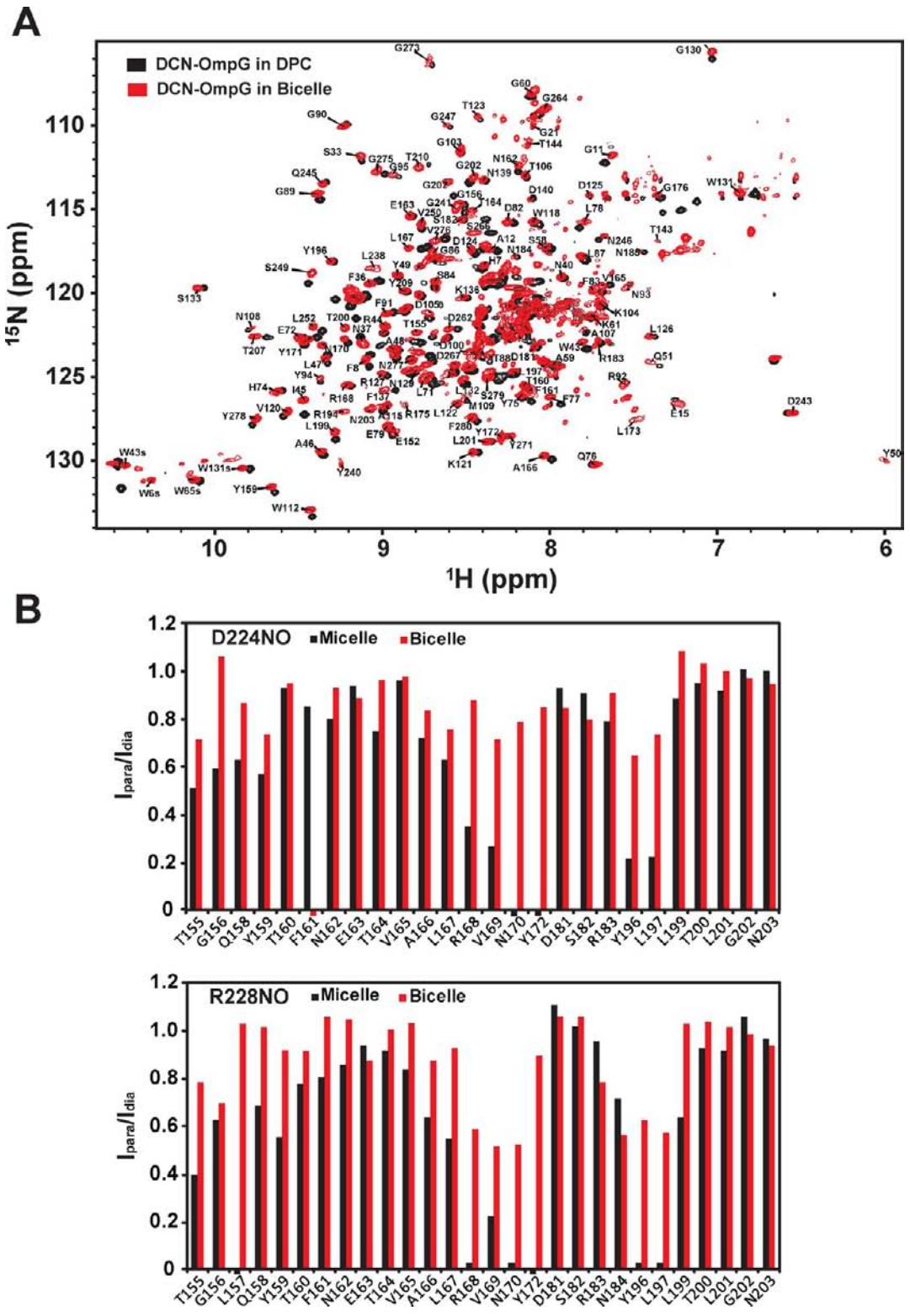

Figure 6. (A) $^{1}H-^{15}N$ TROSY spectra of ^{2}H-, ^{13}C-, ^{15}N-OmpG in 150 mM DPC micelles and 200 mM 11% (w/v) bicelles (DMPC:DHPC = 1:3). Samples (0.5 mM protein) were prepared in 25 mM bis-Tris, 50 mM NaCl, 0.1 mM EDTA, 0.05% NaN_3, pH 6.3 buffer with appropriate amounts of DPC or bicelles. The assignments were obtained as described in the text. (B) Comparison of intensity ratios I_{para}/I_{dia} of barrel residues in 155−203 region of OmpG affected by nitroxide-labeled OmpG D224NO (top panel) and R228NO (bottom panel) in DPC micelles (black bars) and DMPC:DHPC bicelles (red bars). Small negative bars signify data not available. Small positive bars signify $I_{para}/I_{dia} = 0$.

lipids shifted some, but not many peaks in the TROSY spectra, indicating only minor structural changes. Whatever these minor changes may be, they are not specific to LPS because the same shifts were produced by LPS and LMPG.

Conformational Analysis of Loops by Disulfide Cross-Linking and Mass Spectrometry. The low pH crystal structure of OmpG indicated that loop 6 folded into the lumen of the pore. Our ensemble conformer 1 resembled this closed

dx.doi.org/10.1021/ja408206e | J. Am. Chem. Soc. 2013, 135, 15101−15113

state of OmpG with loop 6 entering the pore lumen. Loop 6 also had a high chance of interacting with loops 2 and 4 in this ensemble conformer. In order to check whether this predicted close proximity could be validated biochemically, we attempted to capture transiently interacting residues by intramolecular disulfide cross-linking.[34]

Cysteines were first introduced into loops 1 (Y22C), 2 (S58C), 4 (L141C), 5 (S182C), and 6 (I226C) (Figure 7A).

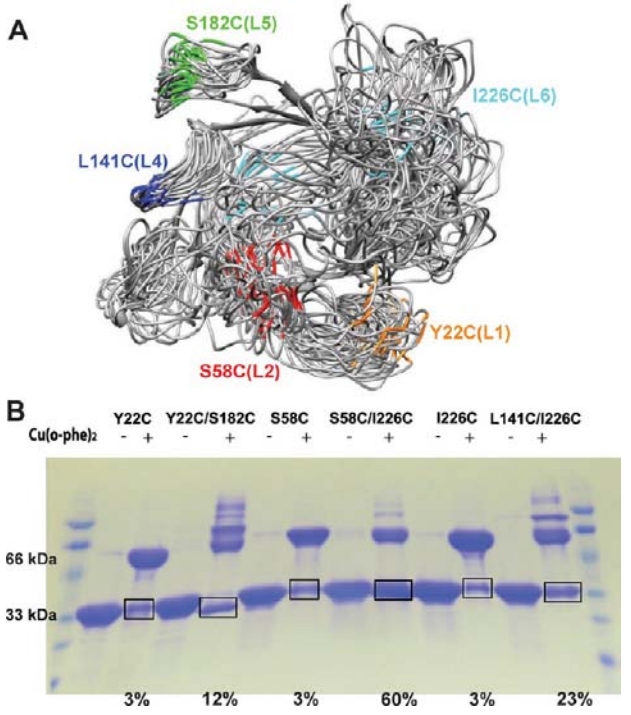

Figure 7. (A) The 15 lowest-energy ensemble structures (N = 3) of OmpG in DPC micelles at pH 6.3. Single Cys mutants in five extracellular loops that were used for disulfide cross-linking are highlighted. (B) SDS-PAGE of single- and double-cysteine mutants before and after treatment with copper phenanthroline, which catalyzes disulfide formation between nearby cysteines. All samples were boiled at 100 °C for 5 min before loading on the gel. First and last lanes are standards, all others are labeled at top. The fractions of monomer bands at 33 kDa were quantified by densitometry, and the respective results are indicated at the bottom of the gel.

We next prepared the double-cysteine mutants S58C/I226C and L141C/I226C to examine whether loop 6 interacted with loops 2 and 4, respectively, by forming intramolecular disulfide bonds cross-linking the respective loops. As a control, double mutant Y22C/S182C was also generated to look for cross-linking of loops 1 and 5, which are predicted from the PRE ensemble calculations not to interact (Figure 7A). Disulfide bond formation was catalyzed by copper phenanthroline and analyzed by SDS-PAGE. Figure 7B shows the cross-linking profiles of Y22C/S182C, S58C/I226C, and L141C/I226C and the corresponding single-cysteine mutants. As expected, the single-cysteine mutants formed only intermolecular disulfide bonds in the presence of copper phenanthroline, represented by the strong dimer band at 66 kDa. The monomer bands at 33 kDa were relatively weak under these conditions. Densitometry shows that the monomer/(monomer + dimer) ratio was only ~3% for all single Cys mutants. In marked contrast, S58C/I226C showed a high population (~60%) of monomer that was presumably intramolecularly cross-linked and only a smaller fraction (~40%) of intermolecularly cross-linked dimer (Figure 7B). No higher order oligomers were observed for this mutant. The L141C/I226C double mutant was intermediate. The monomer band accounted for ~23%, while the dimer fraction was larger and the higher order oligomer fraction was relatively small. The double-cysteine control mutant Y22C/S182C formed predominantly intermolecular disulfide bonds including between dimers and higher order oligomers, suggesting that the distance between loops 1 and 5 was too large for intramolecular cross-linking. Quantification of the monomer and dimer populations by size-exclusion chromatography confirmed the gel densitometry results (Supporting Figure 5). We could exclude the possibility that the monomer bands after copper phenantroline treatment represented unreacted proteins because we were unable to detect any remaining free thiols after reaction with Ellman's reagent and measurement of the absorbance at 412 nm.[35]

To further confirm that the copper phenanthroline-treated monomers were actually intramolecularly cross-linked, their bands were cut out from the SDS-PAGE gels and subjected to trypsin treatment and mass spectrometric analysis. Supporting Figure 6 shows that tryptic fragments with the expected disulfide bonds were generated from the oxidized S58C/I226C and L141C/I226C double mutants. Supporting Table 1 shows that 91% and 86% of all cysteines originated from oxidized S58C-SS-I226C and L141C-SS-I226C tryptic peptides, respectively, proving that the majority of the cysteines in these two double mutants were intramolecularly cross-linked. Since disulfide cross-links require the C_β-carbons of the participating cysteines to be within ~4 Å from each other,[36] it is clear that our PRE measurements and ensemble calculations effectively captured the large amplitude motions that loops 2, 4, and 6 had to undergo to form the observed disulfide bonds.

Single-Channel Current Measurements on Disulfide Cross-Linked Loop Mutations. To further test whether pore loop dynamics and the resulting disulfide cross-links between loops 2 and 6 could be responsible for the gating of the OmpG pore conductance, we performed single-channel conductance measurements of the S58C/I226C double mutant in its oxidized disulfide and in its reduced free sulfhydryl forms. Figure 8 shows the single-channel recordings of cross-linked S58C/I226C before and after the addition of 5 mM DTT. In the disulfide cross-linked form the single-channel current amplitude was only ~50% of the amplitude of the same mutant in the reduced form. In addition, the open state probability was significantly shifted to the closed state in the presence of the disulfide cross-link (Figure 8D). In the fully open state, wild-type OmpG showed a unitary conductance of 1.3 nS.[8] The closing probability of wild-type, defined as the time in which the conductance falls below 1.3 nS was 10.0 ± 2.7% at −50 mV (Supporting Table 2). The oxidized S58C/I226C opened maximally to 0.6 nS and its closing probability, defined as the time in which the conductance falls below 0.6 nS was 53.2 ± 9.1% at −50 mV. The closing frequency also increased substantially in the cross-linked mutant compared to wild-type (Supporting Table 2). In conclusion, our electrophysiological results support the notion that loop 6 cooperates with loop 2 to gate the activity of the OmpG channel.

Structural Ensemble at pH 7.0. Since the pH titration experiments suggested that several residues of loop 6 changed from the intermediate to the fast exchange regime when the pH was raised from 6.3 to 7.0, we measured the relaxation enhancements with the same 9 nitroxide labels also at pH 7.0

dx.doi.org/10.1021/ja408206e | J. Am. Chem. Soc. 2013, 135, 15101−15113

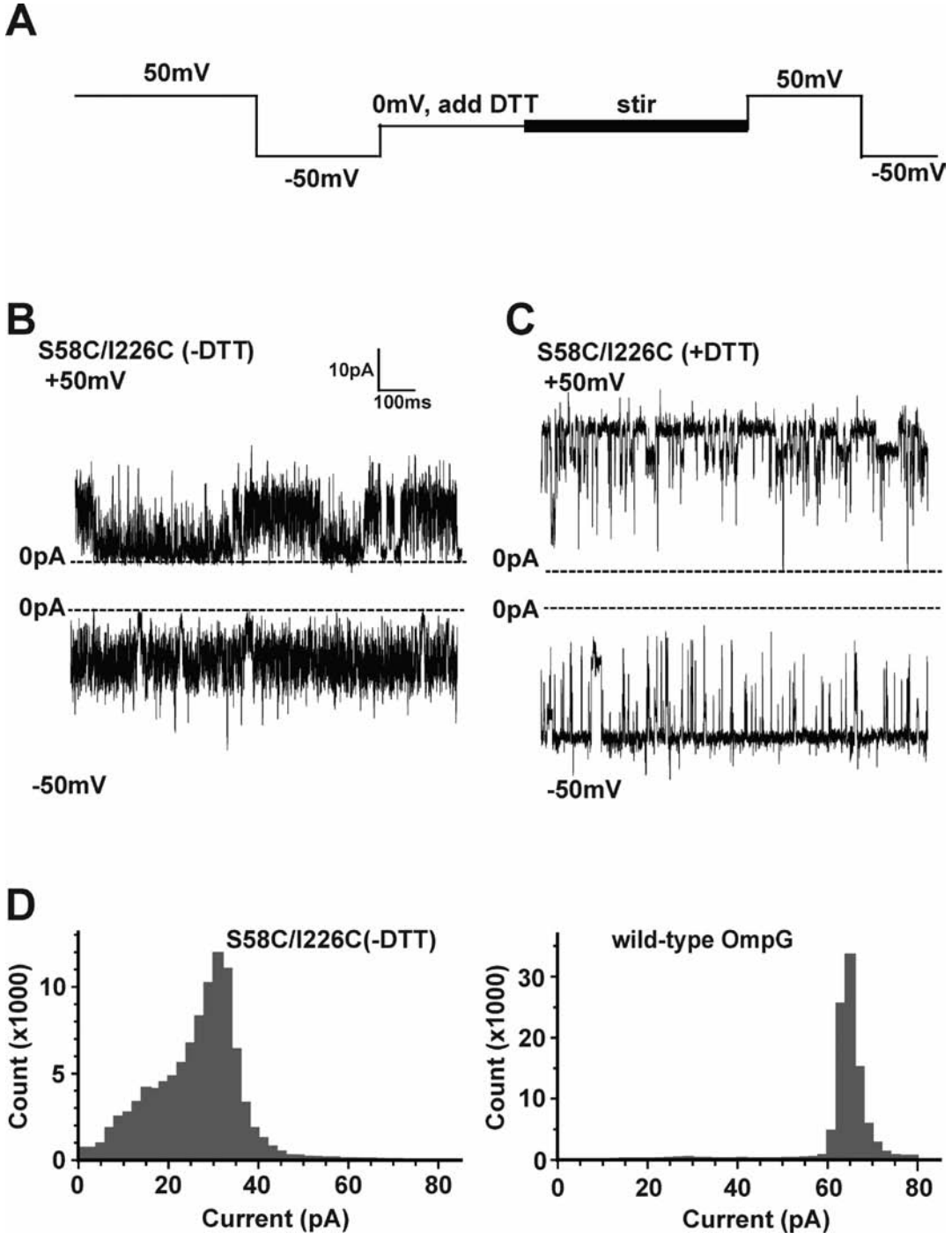

Figure 8. Single-channel current recordings of oxidized and reduced S58C/I226C-OmpG in planar lipid bilayers. (A) Protocol of current recording. Positive (+50 mV) and negative (−50 mV) voltage recordings were followed by reduction with DTT and another cycle of ±50 mV recordings. (B) Typical single-channel current profile of disulfide cross-linked S58C/I226C-OmpG. (C) Typical single-channel current profile of reduced free sulfhydryl S58C/I226C-OmpG. (D) Closing probabilities and frequencies of cross-linked S58C/I226C mutant and wild-type OmpG.

and used the obtained PRE data for similar ensemble calculations. In this case, the ensemble size had to be increased to $N = 4$ to obtain good fits to the PRE data (Figure 4A, red curve). Figure 9 shows the resulting weighted density maps of D224, I226, and R228 at pH 7.0. Three conformers similar to those at pH 6.3 were obtained. The major difference was the additional ensemble conformer 4, which interacted even more with the barrel wall than ensemble conformer 3. The increased intensity of the TROSY peaks in loop 6 at pH 7, compared to pH 6.3 is consistent with a more mobile loop at the higher pH.

Comparison of Loop Dynamics in Micelles and Bicelles and with QuietOmpG. To gain qualitative insight in pH-dependent loop dynamics changes in different environments and with the quiet mutant of OmpG, we performed pH titrations with selectively ^{15}N-isoleucine-labeled proteins reconstituted in the DMPC:DMPS:DHPC = 4:1:15 bicelles and with quietOmpG in a similar fashion, as shown for wild-type in micelles in Figure 2. To monitor the intensity of the loop I226 peak, we normalized it to the rather constant intensity of the central barrel I45 peak in the same spectrum. In

dx.doi.org/10.1021/ja408206e | J. Am. Chem. Soc. 2013, 135, 15101−15113

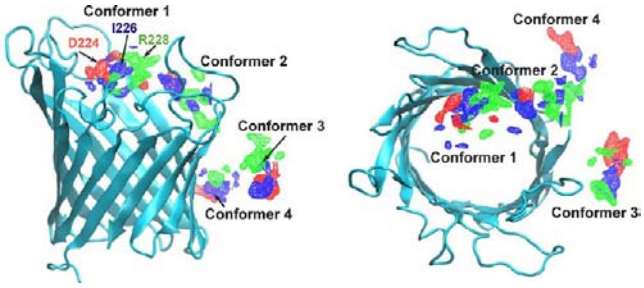

Figure 9. Weighted density maps of D224 (red), I226 (blue), and R228 (green) calculated using the 15 lowest-energy ensemble structures (N = 4) of OmpG in DPC micelles at pH 7.0. The densities partition into four labeled ensemble conformers. Conformers 2 and 4 overlap in the projection view on the right.

DPC micelles the intensity ratio of I226/I45 was 0.25 at pH 6.3 and 7.18 at pH 7.0, which represents a 28-fold increase over this narrow pH range. The same ratios in lipid bicelles were 1.14 and 2.86, respectively, i.e., representing only a 2.5-fold increase from pH 6.3 to 7.0 (Supporting Table 2). When the same comparison was made with a sample of selectively ^{15}N-isoleucine-labeled quietOmpG in DPC, the ratio increased 2.7-fold from 0.99 to 2.64 (Supporting Table 3). These results show that the lipid environment matters for the pH-dependent release of loop 6. They also demonstrate that the loop in quietOmpG appears to be less immobilized at pH 6.3 than in wild-type OmpG.

DISCUSSION

Determining the structure of a protein is very helpful but often not sufficient to explain its function. Sometimes even the availability of two structures, for example, in the on and off states, is still not sufficient to rationalize a protein's function. Rather, distributions of numerous interconverting states need to be invoked to fully understand how an enzyme or structural protein works. The concept of conformational ensembles has been well-accepted for describing states of soluble proteins[37−40] but is a rather new concept to explain functions of integral membrane proteins. This is not surprising because a great many fold-fewer membrane protein structures have been determined than soluble protein structures, and membrane proteins crystallized in two functionally different conformations are exceedingly rare. NMR spectroscopy has been the primary method to examine protein dynamics and to characterize conformational ensembles at high resolution. But, like crystallography, NMR of membrane proteins lags far behind NMR of soluble proteins. Less than 12 structures of larger membrane proteins have been solved thus far by NMR (for reviews, see refs 41−44), and dynamical solution NMR studies on membrane proteins are only emerging.[45−47] The membrane channel OmpG offers a unique opportunity to examine the conformational dynamics of a large membrane protein because: (i) its pore conductance is gated by pH[5,8,9,48−50] and (ii) some of the extracellular loops including the main gating loop 6 are poorly structured and undergoing relatively slow conformational exchange in detergent micelles that were used in solution NMR studies[7] and perhaps in lipid bilayers as shown by atomic force microscopy.[9] Relaxation dispersion experiments have been widely used to characterize the dynamics of chemical exchange and determine the structure of transient and sparse-populated intermediate states.[51−53] However, despite partial success (Supporting Figure 1), it has been difficult to apply relaxation dispersion experiments to characterize the dynamics of the extracellular loops of OmpG because: (i) many residues in these loops were invisible by NMR or gave weak signals and (ii) the chemical shift differences of the residues that were visible by NMR were negligible in the different conformers. We therefore applied a PRE-based ensemble approach to characterize multiple ensemble conformations that explain the pH-dependent opening and closing of the OmpG channel.

Our results show that loop 6, which is the main contributor to the opening and closing of the OmpG pore, is indeed undergoing intermediate exchange under NMR conditions that were used to determine the solution structure of OmpG as has been suspected before.[7] The time regime of conformational exchange can be shifted to some extent by pH for some of the loop residues, as some resonances appear or disappear at high or low pH, respectively. In addition, selective labeling allowed us to assign seven additional residues of OmpG that previously could not be assigned.

The pore conductance of wild-type OmpG is 1.3 nS and fluctuates to smaller values ∼5−10% of the time at pH 8.5 (Figure 8D and Supporting Table 2) and more often at lower values of pH.[3,4] The present work shows that these closing fluctuations can be captured structurally by PRE measurements and corresponding ensemble calculations. At pH 6.3, three conformational ensembles described the experimental data very well (Figure 5). One ensemble resembles the closed structure determined by crystallography at pH 5.6 quite well but is still much more disordered in the loop regions than the single crystal conformer. The second conformational ensemble had its loop regions extended above the barrel wall in a similar but more disordered fashion than in the crystal structure at pH 7.5. We therefore assign this conformational ensemble to the open form of the OmpG channel. The third conformational ensemble seen by NMR does not have a crystallographic counterpart. It is interesting to compare our PRE ensemble structures with the published crystal structures. In Supporting Figure 7 we plot the global backbone RMSDs of our three pH 6.3 conformers together with the B-factors of the pH 5.6 and 7.5 crystal structures. The figure shows that the flexibilities of the loops coincide in the crystal and NMR ensemble structures. As expected, the loop RMSDs are much larger than the barrel RMSDs and coincide with larger B-factors of both crystal structures. Because of the increased number of restraints for the loops, it is also not surprising that all three ensemble structures show much smaller RMSDs in the loops and particularly in the labeled residues than in the NMR structure that was calculated without PREs.

In the third conformational ensemble, loop 6 was folded back onto the micelle surface and presumably interacted with the lipid molecules in the micelle. The notion that loop 6 interacts with lipids in this conformer is supported by PRE measurements in lipid bicelles, which are larger and more disk-shaped lipid structures. When OmpG was embedded into lipid bicelles, loop 6 did not bend as far back in the third conformer as in the micelles (Figure 6), suggesting, again, that it interacted with the lipid surface in these larger, more bilayer-like structures. Charge interactions between loop 6 and the bicelle surface appear not to play a role because essentially the same results were obtained with neutral and negatively charged bicelles. The natural outer membrane lipid LPS also had only a minimal and nonspecific effect on the loop conformation of OmpG in micelles, which is in contrast to the *Pseudomonas aeruginosa* outer membrane protein OprH, which exhibited significant and specific chemical

dx.doi.org/10.1021/ja408206e | J. Am. Chem. Soc. 2013, 135, 15101−15113

shift differences in the presence and absence of LPS.[54] Previous results showed that the gating of OmpG was modulated by the lipid composition of aymmetric bilayers, which also indicated an interaction of the gating loops with membrane lipids.[55] Our micelles and the bilayers formed from lipid bubbles in organic solvent are rather special systems, and more work in other model systems is required to address the question of how the physiological lipid environment of the outer membrane may affect the loop and gating dynamics of OmpG.

Our PRE-based ensemble calculations and particularly the existence of the closed pore ensemble were confirmed by selective disulfide cross-linking experiments. When cysteines were engineered into places in the loops that were predicted from the NMR ensemble calculations to be in close contact, efficient disulfide cross-linking was observed under oxidizing conditions (Figure 7). Loops 2 and 6 were cross-linked, but loops 1 and 5 were not, i.e., exactly as predicted from the ensemble calculations. Cross-links between loops 4 and 6 were also observed, again in close correspondence to the NMR predictions, but were less frequent than cross-links between loops 2 and 6. It should be pointed out that PREs and disulfide cross-linking favor conformations that bring the chemical or NMR probes together. Conformers, in which these probes are far apart, may be underestimated. However, since each nitroxide interacts with many nuclear spins, PREs should sample most relevant conformations.

Despite of its limitation in extracting kinetic details of exchange rate or population,[56] the PRE-based ensemble approach has been essential for characterizing transient interactions in soluble proteins[17,19,57−61] involving domain motions as well as protein−protein and protein−DNA interactions. Ensemble approaches were also applied to characterize intrinsically disordered proteins[62] and a lipid tail-anchored membrane protein.[25] Here we showed that PRE-based ensemble calculations can give accurate pictures of the dynamical distribution of functionally important flexible portions of a large integral membrane protein that functions as a membrane channel. Integral membrane proteins may exhibit more complex dynamic properties compared their soluble counterparts due to their residence in the viscous and highly ordered milieu of the lipid bilayer or micelle/bicelle.

It is not unusual to observe intermediate chemical exchange in membrane proteins, resulting in the complete or partial loss of some of their NMR signals. Structural information from functionally important segments or domains of these proteins is therefore often difficult to obtain. For example, the functionally very important gating loop 6 of OmpG was largely invisible by traditional NMR methods. In the present study, we overcame this problem by demonstrating that the PRE-based approach allowed us to extract conformational ensembles of protein segments that were invisible by NMR methods that only relied on nuclear spins.

We expect this method to become applicable also to the study of many other membrane proteins that exhibit complex dynamical properties and that the approach will help explain the functions of these proteins. This is of course not limited to membrane pores and ion channels. Membrane-bound enzymes, receptors, transporters, and signaling adaptors may exhibit as many intrinsically disordered regions as soluble proteins, but they have not yet been explored in as much detail, mostly because of a lack of appropriate methods. We believe that the PRE ensemble approach, applied here for the first time to a membrane protein, can fill this gap. We expect that many interesting studies on membrane proteins will emerge from applications of this and related NMR methods that will increasingly emphasize the dynamics and gain of structure of membrane proteins.

■ ASSOCIATED CONTENT

Supporting Information

Supporting figures and tables illustrate the ^{15}N relaxation dispersion profiles of selective residues, the intensity ratio of I_{para}/I_{dia} for $^{1}H-^{15}N$ TROSY cross-peaks at eight different nitroxide-labeling sites, the determination of the correlation time of OmpG in bicelles, the effect of LPS and LMPG on OmpG in DPC micelles, the size exclusion elution profiles of S58C/I226C, S58C, and I226C-OmpG after disulfide cross-linking, representative MS/MS spectra of disulfide cross-linked and trypsin-treated monomeric bands of S58C/I226C- and L141C/I226C-OmpG, the global root-mean-square displacement values of the backbone residues averaged over the NMR ensemble and the B-factors of the crystal structures of OmpG in open and closed states, the mass spectrometry analysis of cysteines in their oxidized and reduced forms, the pore closing probabilities and frequencies of wild-type and oxidized S58C/I226C mutant OmpG measured at pH 8.5, and the intensity ratios of I226 over I45 $^{1}H-^{15}N$ TROSY cross-peaks of OmpG and quietOmpG in DPC or bicelles at pH 6.3 and pH 7.0. This material is available free of charge via the Internet at http://pubs.acs.org.

■ AUTHOR INFORMATION

Corresponding Author

E-mail:Lkt2e@ virginia.edu

Notes

The authors declare no competing financial interest.

■ ACKNOWLEDGMENTS

This work was supported by NIH grant R01 GM051329. We thank Dr. Nicolas Sherman from the UVa Biomolecular Research Facility for the performance of the Mass Spectrometry experiments.

■ REFERENCES

(1) Misra, R.; Benson, S. A. *J. Bacteriol.* **1989**, *171*, 4105.
(2) Fajardo, D. A.; Cheung, J.; Ito, C.; Sugawara, E.; Nikaido, H.; Misra, R. *J. Bacteriol.* **1998**, *180*, 4452.
(3) Conlan, S.; Zhang, Y.; Cheley, S.; Bayley, H. *Biochemistry* **2000**, *39*, 11845.
(4) Conlan, S.; Bayley, H. *Biochemistry* **2003**, *42*, 9453.
(5) Yildiz, O.; Vinothkumar, K. R.; Goswami, P.; Kuhlbrandt, W. *Embo J.* **2006**, *25*, 5240.
(6) Subbarao, G. V.; van den Berg, B. *J. Mol. Biol.* **2006**, *360*, 750.
(7) Liang, B. Y.; Tamm, L. K. *Proc. Natl. Acad. Sci. U.S.A.* **2007**, *104*, 16140.
(8) Chen, M.; Khalid, S.; Sansom, M. S. P.; Bayley, H. *Proc. Natl. Acad. Sci. U.S.A.* **2008**, *105*, 6272.
(9) Mari, S. A.; Köster, S.; Bippes, C. A.; Yildiz, Ö.; Kühlbrandt, W.; Müller, D. J. *J. Mol. Biol.* **2010**, *396*, 610.
(10) Liang, B. Y.; Bushweller, J. H.; Tamm, L. K. *J. Am. Chem. Soc.* **2006**, *128*, 4389.
(11) Beel, A. J.; Mobley, C. K.; Kim, H. J.; Tian, F.; Hadziselimovic, A.; Jap, B.; Prestegard, J. H.; Sanders, C. R. *Biochemistry* **2008**, *47*, 9428.
(12) Chen, H. L.; Ji, F.; Olman, V.; Mobley, C. K.; Liu, Y. Z.; Zhou, Y. P.; Bushweller, J. H.; Prestegard, J. H.; Xu, Y. *Structure* **2011**, *19*, 484.

(13) Zhuang, T. D.; Jap, B. K.; Sanders, C. R. *J. Am. Chem. Soc.* **2011**, *133*, 20571.
(14) Van Horn, W. D.; Beel, A. J.; Kang, C. B.; Sanders, C. R. *Biochim. Biophys. Acta, Biomembr.* **2010**, *1798*, 140.
(15) Anthis, N. J.; Doucleff, M.; Clore, G. M. *J. Am. Chem. Soc.* **2011**, *133*, 18966.
(16) Clore, G. M. *Protein Sci.* **2011**, *20*, 229.
(17) Iwahara, J.; Clore, G. M. *Nature* **2006**, *440*, 1227.
(18) Tang, C.; Louis, J. M.; Aniana, A.; Suh, J. Y.; Clore, G. M. *Nature* **2008**, *455*, 693.
(19) Tang, C.; Ghirlando, R.; Clore, G. M. *J. Am. Chem. Soc.* **2008**, *130*, 4048.
(20) Clore, G. M.; Iwahara, J. *Chem. Rev.* **2009**, *109*, 4108.
(21) Clore, G. M.; Tang, C.; Iwahara, J. *Curr. Opin. Struct. Biol.* **2007**, *17*, 603.
(22) Waugh, D. S. *J. Biomol. NMR* **1996**, *8*, 184.
(23) Long, D.; Liu, M. L.; Yang, D. W. *J. Am. Chem. Soc.* **2008**, *130*, 17629.
(24) Bieri, M.; Gooley, P. R. *BMC Bioinformatics* **2011**, *12*, 421.
(25) Liu, Y. Z.; Kahn, R. A.; Prestegard, J. H. *Nat. Struct. Mol. Biol.* **2010**, *17*, 876.
(26) Iwahara, J.; Schwieters, C. D.; Clore, G. M. *J. Am. Chem. Soc.* **2004**, *126*, 5879.
(27) Solomon, I. *Phys. Rev.* **1955**, *99*, 559.
(28) Bloembergen, N. *J. Chem. Phys.* **1957**, *27*, 572.
(29) *Paramagnetic Constraints in Structure Determination*; http://www.nmr2.buffalo.edu/nesg.wiki/Paramagnetic_Constraints_in_Structure_Determination (accessed April 17, 2013).
(30) Schwieters, C. D.; Kuszewski, J. J.; Tjandra, N.; Clore, G. M. *J. Magn. Reson.* **2003**, *160*, 65.
(31) Schwieters, C. D.; Kuszewski, J. J.; Clore, G. M. *Prog. Nucl. Magn. Reson. Spectrosc.* **2006**, *48*, 47.
(32) Schwieters, C. D.; Clore, G. M. *J. Biomol. NMR* **2002**, *23*, 221.
(33) Lee, D.; Hilty, C.; Wider, G.; Wüthrich, K. *J. Magn. Reson.* **2006**, *178*, 72.
(34) Hong, H.; Szabo, G.; Tamm, L. K. *Nat. Chem. Biol.* **2006**, *2*, 627.
(35) Ellman, G. L. *Arch. Biochem. Biophys.* **1959**, *82*, 70.
(36) Careaga, C. L.; Falke, J. J. *Biophys. J.* **1992**, *62*, 209.
(37) Sadqi, M.; Casares, S.; Abril, M. A.; Lopez-Mayorga, O.; Conejero-Lara, F.; Freire, E. *Biochemistry* **1999**, *38*, 8899.
(38) Pan, H.; Lee, J. C.; Hilser, V. J. *Proc. Natl. Acad. Sci. U.S.A.* **2000**, *97*, 12020.
(39) Boehr, D. D.; Nussinov, R.; Wright, P. E. *Nat. Chem. Biol.* **2009**, *5*, 789.
(40) Jamros, M. A.; Oliveira, L. C.; Whitford, P. C.; Onuchic, J. N.; Adams, J. A.; Jennings, P. A. *PLoS Comput. Biol.* **2012**, *8*, e1002695.
(41) Tamm, L. K.; Liang, B. Y. *Prog. Nucl. Magn. Reson. Spectrosc.* **2006**, *48*, 201.
(42) Hiller, S.; Wagner, G. *Curr. Opin. Struct. Biol.* **2009**, *19*, 396.
(43) Kim, H. J.; Howell, S. C.; Van Horn, W. D.; Jeon, Y. H.; Sanders, C. R. *Prog. Nucl. Magn. Reson. Spectrosc.* **2009**, *55*, 335.
(44) Opella, S. J. *Ann. Rev. Anal. Chem* **2013**, *6*, 305.
(45) Hwang, P. M.; Choy, W. Y.; Lo, E. I.; Chen, L.; Forman-Kay, J. D.; Raetz, C. R. H.; Prive, G. G.; Bishop, R. E.; Kay, L. E. *Proc. Natl. Acad. Sci. U.S.A.* **2002**, *99*, 13560.
(46) Liang, B.; Arora, A.; Tamm, L. K. *Biochim. Biophys. Acta, Biomembr.* **2010**, *1798*, 68.
(47) Chill, J. H.; Naider, F. *Curr. Opin. Struct. Biol.* **2011**, *21*, 627.
(48) Korkmaz, F.; Köster, S.; Yildiz, Ö.; Mäntele, W. *Spectrochim. Acta, Part A* **2012**, *91*, 395.
(49) Korkmaz-Özkan, F.; Köster, S.; Kühlbrandt, W.; Mäntele, W.; Yildiz, Ö. *J. Mol. Biol.* **2010**, *401*, 56.
(50) Damaghi, M.; Bippes, C.; Köster, S.; Yildiz, Ö.; Mari, S. A.; Kühlbrandt, W.; Müller, D. J. *J. Mol. Biol.* **2010**, *397*, 878.
(51) Palmer, A. G. *Chem. Rev.* **2004**, *104*, 3623.
(52) Korzhnev, D. M.; Kay, L. E. *Acc. Chem. Res.* **2008**, *41*, 442.
(53) Osawa, M.; Takeuchi, K.; Ueda, T.; Nishida, N.; Shimada, I. *Curr. Opin. Struct. Biol.* **2012**, *22*, 660.
(54) Edrington, T. C.; Kintz, E.; Goldberg, J. B.; Tamm, L. K. *J. Biol. Chem.* **2011**, *286*, 39211.
(55) Hwang, W. L.; Chen, M.; Cronin, B.; Holden, M. A.; Bayley, H. *J. Am. Chem. Soc.* **2008**, *130*, 5878.
(56) Kleckner, I. R.; Foster, M. P. *Biochim. Biophys. Acta, Proteins Proteomics* **2011**, *1814*, 942.
(57) Bermejo, G. A.; Strub, M. P.; Ho, C.; Tjandra, N. *Biochemistry* **2010**, *49*, 1893.
(58) Tang, C.; Schwieters, C. D.; Clore, G. M. *Nature* **2007**, *449*, 1078.
(59) Cordina, N. M.; Liew, C. K.; Gell, D. A.; Fajer, P. G.; Mackay, J. P.; Brown, L. J. *Protein Sci.* **2012**, *21*, 1376.
(60) Volkov, A. N.; Ubbink, M.; van Nuland, N. A. J. *J. Biomol. NMR* **2010**, *48*, 225.
(61) Tang, C.; Iwahara, J.; Clore, G. M. *Nature* **2006**, *444*, 383.
(62) Huang, J. R.; Grzesiek, S. *J. Am. Chem. Soc.* **2010**, *132*, 694.